

## Deep *HST* *V*- and *I*-Band Observations of the Halo of M31: Evidence for Multiple Stellar Populations<sup>1</sup>

Stephen Holland, Gregory G. Fahlman, & Harvey B. Richer

Department of Physics & Astronomy

#129–2219 Main Mall

University of British Columbia

Vancouver, B.C., Canada

V6T 1Z4

### ABSTRACT

We present deep ( $V \simeq 27$ ) *V*- and *I*-band stellar photometry obtained using the *Hubble Space Telescope*'s WFPC2 in two fields in the M31 halo. These fields are located 32' and 50' from the center of M31 approximately along the SE minor axis at the locations of the M31 globular star clusters G302 and G312 respectively. The M31 halo luminosity functions are not consistent with a single high-metallicity population but are consistent with a mix of 50% to 75% metal-rich stars and 25% to 50% metal-poor stars. This is consistent with the observed red giant branch morphology, the luminosity of the horizontal branch, and the presence of RR Lyrae stars in the halo of M31. The morphology of the red giant branch indicates a spread in metallicity of  $-2 \lesssim [m/H] \lesssim -0.2$  with the majority of stars having  $[m/H] \simeq -0.6$ , making the halo of M31 significantly more metal-rich than either the Galactic halo or the M31 globular cluster system. The horizontal branch is dominated by a red clump similar to the horizontal branch of the metal-rich Galactic globular cluster 47 Tuc but a small number of blue horizontal branch stars are visible, supporting the conclusion that there is a metal-poor component to the stellar population of the halo of M31. The number of blue horizontal stars is smaller than would be expected from the observed metallicity distribution but it is not clear if this is due to the photometric limits of our data or a second parameter effect in the halo of M31. We find a lower limit to the helium abundance of  $Y \simeq 0.20$  to 0.27, comparable with the Galactic value. Luminosity functions show weak evidence that the  $R_{M31} = 50'$  field contains a higher fraction of metal-poor stars than the  $R_{M31} = 32'$  field but the metallicity distributions of the RGB stars in each field strongly suggest that both fields have the same mix of stellar populations.

---

<sup>1</sup>Based in observations with the NASA/ESA *Hubble Space Telescope*, obtained at the Space Telescope Science Institute, which is operated by the Association of Universities for Research in Astronomy, Inc., under NASA contract NAS5-26555.

*Subject headings:* galaxies: individual (M31) — galaxies: stellar content — stars: luminosity function

## 1. Introduction

The stellar populations in the halo of the Andromeda Galaxy (M31 = NGC 224) provide a direct tracer of the star formation history, and the early evolution, of that galaxy. M31 is approximately twice as massive as, and slightly more metal-rich than, the Milky Way. It is our nearest large galactic neighbor and has a similar Hubble type so M31 is generally regarded as being a twin of our Galaxy. The low inclination ( $i = 12^\circ.5$ , Hodge 1992) makes it possible to study the stellar halo with minimal contamination from disk stars.

The earliest published color-magnitude diagrams (CMDs) of the M31 halo were obtained by Crotts (1986) and Mould & Kristian (1986). Mould & Kristian (1986) studied a field  $\sim 7$  kpc from the center of M31 along the SE minor axis and found a mean metallicity of  $[\overline{\text{Fe}/\text{H}}] \sim -0.6$ , comparable to that of the metal-rich Galactic globular star cluster (GC) 47 Tuc. Subsequent ground-based studies by Pritchett & van den Bergh (1988), Christian & Heasley (1991), Davidge (1993), Durrell et al. (1994), and Couture et al. (1995) produced CMDs reaching down to near the level of the horizontal branch (HB) stars. These studies confirmed that the M31 halo has a mean metallicity similar to that of 47 Tuc, making the M31 halo significantly more metal-rich than the Galactic halo. Several of these studies have shown that the observed spread in color across the red giant branch (RGB) is larger than what would be expected from photometric uncertainties and thus could be due to an intrinsic spread in the metallicity of the halo of M31 ( $0.3 \lesssim \sigma_{[\text{m}/\text{H}]} \lesssim 0.5$ ). A deep  $V$ - and  $I$ -band study of the halo of M31 in the vicinity of five of M31's GCs by Couture et al. (1995) found that the halo was dominated by a stellar population with a mean metallicity comparable to that of 47 Tuc but that a small component of the RGB stars had  $[\text{Fe}/\text{H}] \simeq -1$  to  $-1.5$ . This is consistent with the presence of the RR Lyrae variables in the halo of M31 as observed by Pritchett & van den Bergh (1987). Recently Rich et al. (1996) used the *Hubble Space Telescope* (*HST*) to obtain CMDs and luminosity functions (LFs) of the metal-rich M31 GC Mayall II (= G1) and the field near it. They found that the halo LF was steeper than the G1 LF and had a less pronounced HB. They compared their M31 halo LF to LFs of several Galactic GCs covering a range of metallicities and found that no single-metallicity LF could reproduce the M31 halo LF.

Deep CMD studies have the potential to provide direct information on the chemical composition and age of the halo of M31. This is important as there is some debate as to the ages of the GCs in the M31 system. There is considerable evidence that the halo of M31 is an old stellar system. Firstly, integrated colors (Frogel et al. 1980, Bohlin et al. 1993) and CMDs suggest that the M31 GC system has an age comparable to that of the Galactic GC system. Secondly, no

extended giant branch of AGB stars has been detected in the halo or the bulge of M31 (Rich & Mighell 1995) as would be expected if an intermediate age population was present. Thirdly, the presence of RR Lyrae variables implies that at least part of the stellar population is old. On the other hand, measurements of  $H\beta$  enhancements (Burstein et al. 1984, Tripicco 1989) in spectra of M31 GCs relative to spectra of Galactic GCs have led to speculation that the M31 GCs could contain a higher fraction of main-sequence stars than the Galactic GCs do, implying that the GCs are younger than their Galactic counterparts. It has recently been suggested (e.g. Faber 1995) that  $H\beta$  enhancements in red elliptical galaxies are due to the presence of a population of young main-sequence turn-off stars. It is, therefore, of great interest to obtain CMD-based determinations of the mix of ages and metallicities in the nearest population of stars resembling a “red elliptical” galaxy—the halo of M31.

Ashman & Bird (1993) identified several distinct groups of GCs in the M31 system which may be associated with sub-structure in the stellar halo of M31. This is similar to the situation in the Galactic halo where several GCs are believed to have originated in external galaxies that are orbiting, or have been accreted by, the Galaxy (e.g. Lin & Richer 1992, Ibata et al. 1994). If accretion has played a significant role in adding material to the halo of M31 then stars from different accretion events could have different ages and metallicities resulting in the M31 halo resembling a patchwork of different stellar populations. Any such clumps in the M31 halo will be seen in projection against the rest of the halo so a CMD will show features from both the underlying halo population and the population of the clump. If the halo of M31 is made up of accreted clumps then CMDs of the halo will show evidence of multiple populations. The exact mix of stellar populations will vary from one accreted clump to the next.

This paper presents deep ( $V \simeq 27$ )  $V$ - and  $I$ -band photometry in two fields  $32'$  and  $50'$  from the center of M31 approximately along the SE minor axis. These fields are at projected distances of 7.6 kpc and 10.8 kpc respectively from the center of M31 assuming a distance modulus of  $\mu = 24.3$  (van den Bergh 1991). This location in the M31 halo is roughly analogous to the distance from the center of the Milky Way to the Sun.

## 2. Observations and Data Reductions

### 2.1. Observations

We obtained deep  $V$ - and  $I$ -band images of the halo of M31 in the vicinity of two bright GCs, G302 ( $\alpha_{2000.0} = 00^{\text{h}}45^{\text{m}}25^{\text{s}}.2$ ,  $\delta_{2000.0} = +41^{\circ}05'30''$ ) and G312 ( $\alpha_{2000.0} = 00^{\text{h}}45^{\text{m}}58^{\text{s}}.8$ ,  $\delta_{2000.0} = +40^{\circ}42'32''$ ). This data was obtained using the *HST* as part of a project (cycle 5 program #5609) to study the internal structures and stellar populations of GCs in M31 (Holland et al. 1996). Table 1 lists the exposures obtained in each filter. Exposure times were selected to avoid saturating the cores of the two GCs being imaged. The total exposure times were 4320 seconds in the F555W (WFPC2 broadband  $V$ ) filter and 4160 seconds in the

F814W (WFPC2 broadband *I*) filter for each field. The data was processed through the standard STScI pipelines. Known bad pixels were masked, and geometric corrections were applied using standard techniques.

The G302 field is located  $32'$  ( $R_{M31} = 7.6$  kpc) from the center of M31 approximately along the SE minor axis while the G312 field is located  $50'$  ( $R_{M31} = 10.8$  kpc) from the center of M31 approximately along the SE minor axis. Each GC was centered on the WF3 CCD leaving the WF2 and WF4 CCDs to image the halo of M31. The tidal radii ( $r_t$ ), determined by fitting Michie–King models (Michie 1963, King 1966) to the surface brightness profiles of G302 and G312, are  $r_t \simeq 10''$  (Holland 1997). Grillmair et al. (1995) found evidence for extra-tidal tails, extending to  $\gtrsim 2r_t$  to  $3r_t$ , in several Galactic GCs. Holland (1997) found weak evidence for stellar density enhancements out to  $\sim 2r_t$  in some M31 GCs including G302 and G312. Since the GCs are located approximately  $40''$  ( $\sim 4r_t$ ) from the edge of the WF3 CCD the WF2 and WF4 CCDs should contain little, if any, contamination from an extended halo of GC stars.

## 2.2. Data Reductions

Photometry was performed on stars imaged by the WFPC2’s WF2 and WF4 CCDs using the DAOPHOT II/ALLFRAME software (Stetson 1987, Stetson 1994). All nineteen images for each field were re-registered to a common coordinate system and median-combined. This served to eliminate cosmic ray hits and to increase the signal-to-noise ratio (S/N) allowing fainter stars to be detected. A square median-filter was run over the combined image to determine large-scale gradients. This smoothed image was then subtracted from the combined image and a constant sky added back to produce a median-subtracted image. This was done so that the star lists and photometry from the halo fields would be obtained in exactly the same manner as the star lists and photometry of the GC stars on the WF3 CCD (see Holland et al. 1996). The size of the square median-filter was  $\sim 5$  times the stellar full-width at half-maximum (FWHM) to avoid smoothing out structure in the stellar images. The DAOPHOT FIND routine with a FIND threshold of  $7.5\sigma_{\text{sky}}$  was used to detect peaks on the median-subtracted image. We experimented with different FIND thresholds and found that  $7.5\sigma_{\text{sky}}$  excluded most of the mis-identifications of noise spikes & cosmic ray events as stars at faint magnitudes while including almost all of the stars down to near the photometric limit of the data. The resulting list of stellar candidates was used as input to ALLFRAME. ALLFRAME does simultaneous point-spread function (PSF) fitting on all the *original* images (*not* the combined median-subtracted image) to preserve the photometric properties of the data. The PSFs used (Stetson 1996) were Moffatians (Moffat 1969) with  $\beta = 1.5$  and a look-up table of residuals. The PSFs varied quadratically over each WF CCD. Only stars that appeared in at least 7 frames in each filter were considered to be real stars.

Aperture corrections were obtained for each CCD in the following manner. First a set of  $\sim 50$  bright isolated stars was selected on each of the WF2 and WF4 CCDs and all remaining stars were subtracted from these images. Next, the total magnitude in an aperture with a  $0''.5$  radius

(Holtzman et al. 1995b) was measured for each star. Aperture corrections were defined in the sense  $\Delta v = v_{\text{ap}} - v_{\text{PSF}}$  for each of the isolated stars. We discarded any star with a combined photometric uncertainty of  $\sqrt{\sigma_{\text{ap}}^2 + \sigma_{\text{PSF}}^2} > 0.14$ , which corresponds to  $S/N \simeq 10$  for each of the aperture and PSF magnitudes. The size of the aperture correction should be independent of magnitude so a plot of  $v_{\text{ap}}$  vs  $v_{\text{PSF}}$  (see Fig. 1) should yield a slope of unity with a zero-point offset corresponding to the value of the aperture correction. However, the WF CCDs suffer from considerable cosmic ray contamination that may bias the observed aperture magnitudes towards brighter magnitudes. In addition the presence of background galaxies and undetected faint stars can bias the  $v_{\text{ap}} - v_{\text{PSF}}$  relation away from a slope of unity. To correct for this we plotted the PSF-magnitudes as a function of the aperture-magnitudes for each WF CCD and iteratively discarded stars that biased the best-fitting straight line away from a slope of unity until the slope approached unity and discarding additional stars failed to drive the slope closer to unity. The aperture correction was then computed from the sample of stars that survived this culling process. Table 2 lists the adopted aperture corrections for the WF2 and WF4 CCDs. Fig. 1 shows the residuals for the  $I$ -band aperture corrections to the WF2 CCD in the G312 field.

The photometry was calibrated to standard Johnson–Cousins  $V$ - and  $I$ -band magnitudes using the transformations of Holtzman et al. (1995b). A charge transfer efficiency correction of 2% (Holtzman et al. 1995a) was adopted and a reddening of  $E_{B-V} = 0.08 \pm 0.02$  (Burstein & Heiles 1982) was used. We converted  $E_{B-V}$  to  $E_{V-I}$  using the relationship of Bessell & Brett (1988):  $E_{V-I} = 1.25E_{B-V} = 0.10 \pm 0.03$ , and adopted a distance modulus of  $\mu = (m - M)_0 = 24.3 \pm 0.1$  (van den Bergh 1991). This value agrees well with other M31 distance moduli obtained using Population II distance indicators. Pritchett & van den Bergh (1987) found  $\mu = 24.34 \pm 0.15$  from RR Lyrae variables in the halo of M31 while Christian & Heasley (1991) found  $\mu \sim 24.3$  from the brightest red giants in M31 GCs. Studies of Population I distance indicators such as Cepheids (e.g. Freedman & Madore 1990) and carbon stars (e.g. Brewer et al. 1995) find  $\mu \simeq 24.4$ , slightly larger than the Population II value. We have adopted the lower distance modulus since the halo of M31 appears to consist of Population II stars.

Any stars for which ALLFRAME returned a  $\chi_{\text{DAO}} > 2$  were discarded. The  $\chi_{\text{DAO}}$  value represents the ratio of the observed pixel-to-pixel scatter in the fitting residuals to the expected scatter. Values that are significantly different from unity indicate that an image was not well fit by the stellar PSF. We used an interactive approach to cull the star lists based on the uncertainty in the calibrated magnitudes. A plot of uncertainty vs magnitude was made and a locus defined that corresponded to the expected increase in photometric uncertainty as the stars became fainter. Any stars that were judged to have a significantly greater uncertainty than the typical value for that magnitude was removed. Visual examinations of the CMDs and the WF images suggested that we did not remove legitimate stars from our sample. We wish to emphasize that this culling was done *solely* on the basis of the observed photometric uncertainty of each star, not on the star’s location on the CMD or on the CCD. The photometric uncertainties for our culled data are listed in Table 3.

### 3. The Color–Magnitude Diagrams

#### 3.1. Contamination in the Field

Figs. 2 and 3 show the  $(I, (V - I)_0)$  CMDs for the halo fields around the M31 GCs G302 and G312 respectively. No culling has been applied to these CMDs beyond that done to identify real stellar images as described in Sec. 2.2. The CMD has been dereddened and corrected for interstellar absorption. The reader is referred to Holtzman et al. (1995b) for details on the corrections for interstellar absorption.

The CMDs of the M31 halo will contain contamination from Galactic halo stars. Galactic M-dwarfs have colors of  $(V - I) \sim +1.5$  to  $+3$  so they will appear to the red of the RGB while main-sequence stars and HB stars in the Galaxy will appear to the blue of M31’s RGB. Star count models in the direction of M31, from Ratnatunga & Bahcall (1985), suggest that there will be  $\sim 14 \pm 4$  stars redder than the RGB and  $\sim 1 \pm 1$  stars bluer than the RGB between  $21 \leq V \leq 27$  in each of our fields. Galactic field star contamination, therefore, contributes only  $\sim 0.2\%$  to the total number of stars observed in the G302 field and  $\sim 0.7\%$  to the G312 field. The blue end of the HB is sparsely populated but only  $1 \pm 1$  foreground stars are expected on the blue side of the RGB so uncertainties due to photometric scatter will dominate over the effects of contamination. The small number of Galactic stars expected in our fields means that foreground contamination is not a problem.

Some faint background galaxies may have been mis-identified as stars. The deep galaxy counts of Smail et al. (1995) suggest that  $19 \pm 2$  background galaxies with  $20 \leq I \leq 24$  and  $168 \pm 20$  galaxies with  $24 \leq I \leq 27$  should be located in each of our two fields. Typical galaxies have colors of  $(V - I) \simeq 1.0$  so background galaxies are indistinguishable from stars in a CMD. The small expected number of galaxies with  $I \leq 24$  suggests that background galaxies are not making a significant contribution to the morphology of the RGB. The blue end of the HB is  $\sim 1$  magnitude bluer than typical background galaxies so we believe that the blue HB is not significantly contaminated by galaxies. The galaxy counts suggest that for  $I > 24$  background galaxies make up at most  $2.9\% \pm 0.3\%$  of the objects on the G302 field CMD. In the G312 field background galaxies can account for up to  $10.4\% \pm 1.2\%$  of the objects on the CMD. DAOPHOT/ALLFRAME will discard objects that are not morphologically similar to the stellar PSF for the frame in question so many of the faint background galaxies will already have been discarded. Therefore we believe that mis-identified background galaxies are not significantly biasing the distribution of stars on the CMDs.

A third potential source of contamination is the disk of M31 itself. Mould & Kristian (1986) used the surface photometry of de Vaucouleurs (1958) to estimate that the disk-to-halo ratio in a field  $\sim 35'$  from the center of M31 along the SE minor axis was  $\lesssim 0.014$ . Pritchet & van den Bergh (1988) compared star counts in a field  $40'$  from the center of M31 along the SE minor axis with various models and found that even with a thick disk component the disk-to-halo ratio

would be  $\lesssim 0.04$ . Hodder (1995) adapted the Bahcall & Soneira (1984) Galaxy model to provide star counts and color distributions for an external spiral galaxy and used this model to estimate a disk-to-halo number-density ratio of  $\sim 0.1$  in the G302 field and  $\sim 0.03$  in the G312 field, although these ratios are somewhat dependent on the details of the disk and halo models. Taking the worst-case scenario for disk contamination (that of Hodder 1995) leads us to believe that less than 10% of the stars in the G302 field, and less than 3% in the G312 field, are due to contamination from the disk of M31.

On the basis of these calculations we expect *at most*  $\sim 13\%$  of the objects in each field to be background galaxies or stars that are not members of the M31 halo. Therefore, we conclude that the overall morphologies in our CMDs represent real features in the halo population of M31. The exception is the group of blue objects visible  $\sim 1$  magnitude above the HB in the G302 field (see Fig. 2). A visual examination of the individual CCD frames of the G302 field showed that approximately half of these objects fall on or near background galaxies, saturated stars, or pixels that has been flagged as bad for whatever reasons. The remaining  $\sim 10$  bright blue objects may be nucleated dwarf galaxies, blends of stars, or stars with a large photometric uncertainty.

### 3.2. The Red Giant Branch

The RGBs in the G302 and G312 fields are morphologically similar except for a clump of stars at  $I \sim 23$  in the RGB of the G302 field (see Fig. 2). There is no apparent corresponding clump visible in the G312 field (see Fig. 3). In order to check if this clump is a real feature of the RGB we determined the differential LF for each RGB for  $22 \leq V \leq 24.5$  using a non-parametric histogram. We then constructed a second LF where the clump was removed by interpolating the differential LF across the region containing the clump. The resulting “clumpless” LF was compared to the observed LF using a two-sided two-sample Kolmogorov–Smirnov (K–S) test. This test said that the density enhancement at  $V \sim 24.25$  is significant at less than the  $5 \times 10^{-6}\%$  confidence level, suggesting that the clump in the RGB is not real.

We applied the two-dimensional K–S test (Peacock 1983) to the entire RGB above  $V \geq 24.5$  and found that the RGB stars in the G302 and G312 fields were drawn from the same distributions at the 91% confidence level. The same tests found that the distributions of stars on the blue sides of the upper RGBs ( $V \leq 24$ ,  $(V - I)_0 \leq 1.6$ ) were the same at the 85% confidence level and that the red sides of the upper RGBs ( $V \leq 24$ ,  $(V - I)_0 \geq 1.6$ ) were the same at the 93% confidence level. This is weakly suggestive that the two fields have the same stellar populations.

Figs. 4 and 5 shows the  $(V, (V - I)_0)$  CMDs for the M31 halo fields around G302 and G312 with a series of fiducial sequences of different metallicities added. The three metal-poor fiducial sequences are the RGB ridge lines for the Galactic GCs M15 ( $[m/H] = -2.19$ ), NGC 1851 ( $[m/H] = -1.29$ ), and 47 Tuc ( $[m/H] = -0.71$ ) taken from Da Costa & Armandroff (1990). The two metal rich fiducials are the  $t_0 = 13.8$  Gyr isochrones of Bertelli et al. (1994) with  $[m/H] = -0.4$

and  $[m/H] = 0.0$ . The HB fiducial sequence is that of M54 ( $[m/H] = -1.42$ ) from Sarajedini & Layden (1995).

The observed distribution of stars along the red end of the RGB is consistent with a metal-rich population while the blue side of the RGB is consistent with a low-metallicity population. However, photometry of 47 Tuc (Lee et al. 1977) shows that  $\sim 15\%$  of the stars  $\sim 1$  magnitude brighter than the HB are evolved asymptotic giant branch (AGB) stars. If this ratio holds for the halo of M31 then many of the stars blueward of the  $[m/H] = -1.29$  fiducial sequence will be AGB stars. The spread in metallicity in the RGB stars is clearly visible from the locations of the fiducial sequences. The majority of the stars, however, have  $[m/H] > -0.7$ , consistent with recent studies (see references in Sec. 1) which have found metallicities of  $[m/H] \sim -0.6$  for the halo of M31.

To estimate the contribution to the width of the RGB from the finite depth of the halo we assumed that the projected surface density distribution of stars in the M31 halo follows a de Vaucouleurs  $R^{1/4}$  law,  $\Sigma(R)$ , with an effective radius of  $R_e = 1.3$  kpc and an axial ratio of  $\alpha_s = 0.55$ , in accordance with Pritchett & van den Bergh (1994). The volume density,  $\rho(r)$ , can be obtained from  $\Sigma(R)$ , through Abel’s integral, as follows:

$$\rho(r) = -\frac{1}{\pi} \int_{R=r}^{+\infty} \frac{d\Sigma(R)}{dR} \frac{dR}{\sqrt{R^2 - r^2}} \quad (1)$$

where  $R$  is the projected distance of the field from the center of M31 and  $r$  is the true galactocentric distance of the volume element  $\rho(r)$ .

We computed the density distribution along the line-of-sight at projected distances of  $32'$  and  $50'$  from the center of M31. The spread due to the depth of the halo has a half-power width in  $V$  of  $\sim 0.02$  magnitudes at  $R_{M31} = 32'$  (the G302 field) and  $\sim 0.03$  magnitudes at  $R_{M31} = 50'$  (the G312 field). Changing the effective radius and axial ratio over the ranges found by Hodder (1995) in his study of the structure of M31 does not significantly alter these results. A change of a few hundredths of a magnitude along any of the Da Costa & Armandroff (1990) fiducial RGBs corresponds to a negligible change in color so we conclude that the depth of the M31 halo does not contribute significantly to the observed width of the RGB.

The mean photometric uncertainties in our data are  $\sigma_{V-I} \simeq 0.05$  near the tip of the RGB ( $I \simeq 20$ ) and increase to  $\sigma_{V-I} \simeq 0.10$  at the level of the HB yet the observed spread in color along the RGB is  $\sim 0.5$  magnitudes at the level of the HB and  $\sim 2$  magnitudes near  $I \simeq 20$ . These spreads are too large to be due to photometric uncertainties or the depth of the M31 halo. The turn-over in the RGB near  $V = 23$  is due to the increased opacity from molecular bands as giants expand and become cooler. For shell-hydrogen burning stars with  $[m/H] \gtrsim -1$  the molecular opacity can become high enough to reduce the luminosity of the star so that these stars become fainter as they ascend the RGB. However, Figs. 4 and 5 shows that this flattening will not explain all of the structure in the RGB. Therefore a portion of the width of the RGB is due to an intrinsic spread in the metallicity of the M31 halo stars.



In order to estimate the metallicity distribution of RGB stars we interpolated metallicity values for each star based on the fiducial sequences in Figs. 4 and 5 and the theoretical isochrone of Bertelli et al. (1994) with  $[m/H] = +0.4$  (not plotted). We assumed that the age of the M31 halo is  $t_0 \simeq 14$  Gyr, comparable with the age of the Galactic halo GC system (e.g. Richer et al. 1996). The morphology of the RGB is not sensitive to changes in age of a few Gyr so the exact age adopted for the RGB isochrones is not critical. Fig. 6 shows the probability density distributions of metallicity ( $[m/H]$ ) for RGB stars with  $I < 23$  in the G302 and G312 fields. Based on the photometric uncertainties in our data at the level of the RGB, and the uncertainties inherent in matching theoretical isochrones to observational data, we believe that our metallicity estimates for the RGB stars have uncertainties of  $\sigma_{[m/H]} \sim 0.25$ . A K-S test shows that the two metallicity distributions differ at less than the  $5 \times 10^{-6}\%$  confidence level, strongly suggesting that the stellar populations are the same in both fields. The G302 field distribution has a peak at  $[m/H] = -0.6$  and a FWHM of 1.3 dex while the G312 field distribution has a peak at  $[m/H] = -0.7$  and a FWHM of 1.6 dex. These FWHMs are overestimates of the true metallicity distribution since the probability density distribution function shown in Fig. 6 is essentially a convolution of the data with a unit Gaussian that has a dispersion equal to the uncertainty in a typical measurement. The intrinsic spread in the metallicity can be estimated by deconvolving this Gaussian from the probability density distribution function. This gives an intrinsic FWHM of 1.2 dex for the G302 field and 1.5 dex for the G312 field. The halo stars are clearly more metal-rich than, and have a slightly greater spread in metallicity than, M31 GC system.

The halo metallicity distribution is clearly asymmetric with an extended metal-poor tail. This is partly due to the presence of AGB stars on the blue edge of the RGB and partly due to the metallicities less than  $[m/H] = -2.19$  being extrapolated from the higher-metallicity fiducial sequences. Therefore the shape of the metallicity distribution beyond  $[m/H] \sim -2$  should be regarded with caution. There is a sharp cut-off in the halo metallicity distribution at approximately Solar metallicity. The metal-rich tail of the metallicity distribution drops to zero quite rapidly between  $[m/H] \simeq -0.2$  and  $[m/H] \simeq +0.2$ . A visual examination of the locations of the  $[m/H] = -0.4$  and  $[m/H] = 0.0$  isochrones in Figs. 4 and 5 shows the most metal-rich RGB stars having  $[m/H] \simeq -0.2$  suggesting that the extra-Solar metallicity tail in Fig. 6 is an artifact of the uncertainties in the metallicity determination.

### 3.3. The Horizontal Branch

The HB stars in both fields are concentrated in a red clump between  $0.5 \leq (V - I)_0 \leq 1.0$  with a handful of blue stars between  $0.0 \lesssim (V - I)_0 \leq 0.5$ . The red clump is consistent with what is seen in metal-rich Galactic GCs such as 47 Tuc while the small number of blue HB stars is indicative of a metal-poor population. However, an age spread of  $\sim 5$  Gyr in the halo population could produce a HB morphology similar to what a metallicity spread of  $\sim 1$  dex would produce. This is the classic “second parameter” problem (see van den Bergh 1993, Lee et al. 1994, and

Chaboyer et al. 1996 for recent reviews) affecting the colors of HB stars. The lack of any extended AGB candidates in our data, or in any other M31 halo fields, suggests that a young population ( $\lesssim 5$  Gyr) is not present but there is still the possibility that the M31 halo may contain stars as young as  $\sim 10$  Gyr.

The morphology of the HB in each field can be parameterized by counting the number of red and blue HB stars and computing the HB-ratio =  $(N_B - N_R)/(N_B + N_V + N_R)$  where  $N_B$  is the number of HB stars bluer than the instability strip,  $N_V$  is the number of stars in the instability strip, and  $N_R$  is the number of HB stars redder than the instability strip. Since photometric scatter is quite large ( $\sigma_{(V-I)} \simeq 0.16$ ) at the level of the instability strip, and the instability strip has a width of only  $\sim 0.25$  magnitudes, we did not attempt to identify RR Lyrae candidates. Instead we split the HB at  $(V - I)_0 = 0.5$  and calculated the ratio  $(N_B - N_R)/(N_B + N_R)$ . The G302 field has a HB-ratio of  $-0.91 \pm 0.12$  (Poisson uncertainty) while the G312 field has a HB-ratio of  $-0.92 \pm 0.26$  suggesting that both fields have the same HB morphology. These ratios are lower limits on the actual HR-ratios since the blue HB extends to below the  $\sigma_{(V-I)} = 0.2$  photometric limit suggesting that incompleteness may be causing us to seriously underestimate  $N_B$ . We used the theoretical HBs of Lee et al. (1994) to estimate the expected values of the HB type given the metallicity ratios determined in Sec. 4. The predicted HB-ratios were  $-0.6 \pm 0.3$  in the G302 field and  $-0.1 \pm 0.1$  in the G312 field, somewhat more positive than the values measured from the CMDs. This suggests that either the blue HB suffers from a high degree of incompleteness, or that there is a second parameter contributing to the morphology of the HB in the halo of M31. Detailed incompleteness tests are in progress to attempt to determine whether or not our results are due to the second parameter effect. At present we conclude that the morphology of the HB in the halo of M31 is in broad agreement with the metallicity distribution determined from the RGB morphology but that further work is needed to determine if the lack of blue HB stars (relative to the metallicity spread observed in the RGB stars) is due to photometric limits in our data or a second parameter effect.

The CMDs (Figs. 4 and 5) shows that the HB is not actually horizontal in  $V$ . To estimate the spread in HB magnitudes we split the HB into bins with widths of  $\Delta(V - I) = 0.1$  and fit a sloping Gaussian to the distribution of stars in  $V$  in each bin. The mean width of these Gaussians was  $\sigma_V = 0.14 \pm 0.01$  (standard error) in the G302 field and  $\sigma_V = 0.12 \pm 0.03$  in the G312 field. The mean photometric uncertainty at the level of the red HB is  $\sigma_V = 0.086$ . Subtracting this quadratically from the observed spread in  $V$ -magnitude of the HB gives intrinsic spreads of  $\sigma_V = 0.11 \pm 0.01$  in the G302 field and  $\sigma_V = 0.08 \pm 0.03$  in the G312 field. The finite depth of the halo of M31 also introduces a small broadening in  $V$  (see Sec. 3.2) of the HB. However, this broadening is negligible ( $\sim 3\%$ ) compared with the broadening introduced by photometric uncertainties so it was ignored. The resulting distribution of  $V$ -band magnitudes was converted to iron abundances using the relation of Chaboyer et al. (1996), see below. The derived mean iron abundance is  $[\text{Fe}/\text{H}] = -0.5 \pm 0.6$  (standard deviation) in the G302 field and  $[\text{Fe}/\text{H}] = -0.5 \pm 0.4$  in the G312 field.

The mean magnitude of the red HB stars is  $\bar{V} = 25.18 \pm 0.01$  in the G302 field and  $\bar{V} = 25.17 \pm 0.01$  in the G312 field. These correspond to absolute magnitudes for the HB of  $M_V(HB) = 0.88 \pm 0.1$  in the G302 field and  $M_V(HB) = 0.87 \pm 0.1$  in the G312 field. The relationship between metallicity and absolute magnitudes of RR Lyrae variables,  $M_V(RR)$ , is somewhat uncertain. Chaboyer et al. (1996) find  $M_V(RR) = 0.20[\text{Fe}/\text{H}] + 0.98$ , while Carney et al. (1992) find  $\langle M_V(RR) \rangle = (0.15 \pm 0.01)[\text{Fe}/\text{H}] + (1.01 \pm 0.08)$ . The spread in  $[\text{m}/\text{H}]$  on the RGB, and the observed spread in the magnitude of the red HB stars, allows us to make an estimate of the slope of the metallicity–magnitude relation for HB stars. If we assume that the slope ( $dM_V/d[\text{m}/\text{H}]$ ) is positive and combine the data from both fields to improve the statistics we derive a relationship of  $M_V(HB) = (0.22 \pm 0.02)[\text{m}/\text{H}] + (1.01 \pm 0.11)$ . A preliminary analysis of the CMDs of the M31 GCs G302 and G312 suggests  $M_V(HB) = 0.2[\text{m}/\text{H}] + 1.0$  (see Holland et al. 1996 for details). These results are consistent with the Chaboyer et al. (1996) relation.

The relationship between iron abundance and HB magnitude is very sensitive to the adopted value of the distance modulus. An error of only 0.02 magnitudes in the distance modulus will result in an uncertainty of  $\sim 0.1$  dex in metallicity. Therefore, we believe that the metallicity distribution estimated from the RGB is a better indicator of the mean metallicity of the M31 halo than the metallicity distribution obtained from the HB. However, it should be noted that the metal-poor edge of the HB metallicity distribution ( $\overline{[\text{Fe}/\text{H}]} - 3\sigma_{[\text{Fe}/\text{H}]}$ ) occurs at  $[\text{Fe}/\text{H}] \simeq -2$  in rough agreement with the metallicity distribution of RGB stars. The lack of HB stars with  $[\text{Fe}/\text{H}] \lesssim -2$  supports our conclusion that the metal-poor tail of the RGB metallicity distribution is actually due to calibration uncertainties and contamination of the blue side of the RGB by AGB stars.

The metal-rich edge of the HB metallicity distribution ( $\overline{[\text{Fe}/\text{H}]} + 3\sigma_{[\text{Fe}/\text{H}]}$ ) occurs at  $[\text{Fe}/\text{H}] \simeq +1$ . The RGBs show no evidence for stars with  $[\text{Fe}/\text{H}] \gtrsim -0.2$  so the metal-rich tail in the HB metallicity distribution is most likely an artifact of fitting a Gaussian to a non-Gaussian distribution. In general, red HBs have a well defined faint edge but photometric uncertainties and contamination from RGB stars make it impossible to identify this faint edge in our data. Therefore we conclude that the metal-rich tail of the HB metallicity distribution is spurious.

### 3.4. The Helium Abundance

The helium abundance in the halo of M31 can be estimated from the relative numbers of stars on the HB, the RGB and the AGB,  $R' = N_{\text{HB}}/(N_{\text{RGB}} + N_{\text{AGB}})$  (e.g. Buzzoni et al. 1983). The number of RGB stars brighter than the HB was counted and an estimate of the number of Galactic foreground stars and background galaxies (see Sec. 3.1) was subtracted. The number of HB stars was difficult to estimate since: (1) the blue end of the HB is near the photometric limit of the data, and (2) the red clump of the HB sits on top of the RGB. Since  $N_B$  is small compared with  $N_R$  ( $N_R \sim 0.95N_B$ ), and  $N_B$  remains approximately constant with color bluewards of  $(V - I)_0 \simeq 0.5$ , we believe that the uncertainty in the number of blue HB stars will not

significantly affect the determination of  $N_{\text{HB}}$ . To estimate the degree of contamination in the red clump due to the RGB we interpolated the RGB LF across the HB and subtracted these stars from  $N_{\text{HB}}$ . Since there is confusion between AGB and RGB stars we used the  $R'$  estimator of helium abundance instead of the  $R = N_{\text{HB}}/N_{\text{RGB}}$  estimator.

The resulting ratios are  $R' = 1.37 \pm 0.08$  in the G302 field and  $R' = 0.98 \pm 0.11$  in the G312 field. Using the calibration of Buzzoni et al. (1983) these ratios yield helium abundances of  $Y = 0.27 \pm 0.03$  in the G302 field and  $Y = 0.20 \pm 0.05$  in the G312 field. Our uncertainty estimates only include Poisson uncertainties and an estimate of the uncertainty in our estimate of the RGB contamination in the red clump of the HB. They do not include any potential incompleteness effects at the blue end of the HB. Therefore, our quoted uncertainties should be treated as lower limits on the true uncertainty. Further, the effects of incompleteness as the blue end of the HB may have resulted in our underestimating the number of HB stars and therefore underestimating the helium abundance. Since the G302 field contains  $\sim 4$  times the number of stars as the G312 field we believe that the helium abundance derived from the G302 field CMD is a more reliable estimate of the helium abundance in the halo of M31 than that derived from the G312 field CMD. We note that the two values are in agreement at the  $\sim 1\text{-}\sigma$  level.

A halo helium abundance of  $Y \simeq 0.20$  to  $0.27$  is consistent with the mean helium abundance,  $\bar{Y} = 0.23 \pm 0.02$  (Buzzoni et al. 1983), seen in the blue Galactic globular clusters. Our estimate is slightly less than the helium abundance of 47 Tuc,  $Y = 0.28 \pm 0.04$  (Hesser et al. 1987), however the large uncertainty in our result makes it compatible with that of 47 Tuc. The similarity between the helium abundance of the old Galactic GCs and the halo stars in M31 suggests that the two populations are similar.

#### 4. The Halo Luminosity Function

Preliminary artificial star tests indicate that our photometry is complete to at least the level of the HB ( $V \simeq 25$ ) in both the G302 and G312 fields. This is consistent with the results of Rich et al. (1996) who found that star-counts in the halo of M31 obtained using WFPC2 data were complete to at least  $V \sim 26$ . The  $V$ - and  $I$ -band LFs in each field are tabulated in Table 4. The  $\phi$  values are the number of stars in each field per 0.2 magnitude bin. The total area of each field is  $\sim 3.2\text{arcmin}^2$  after masking and bad pixels are taken into account. Fig. 7 shows the LF for the G302 field compared with LFs for the metal-rich M31 GC G1 (Rich et al. 1996), a theoretical LF for an old ( $t_0 = 14$  Gyr) metal-rich ( $[\text{Fe}/\text{H}] = -0.47$ ,  $[\text{O}/\text{Fe}] = +0.23$ ) population (Bergbusch & Vandenberg 1992), the metal-rich Galactic GC 47 Tuc (Hesser et al. 1987), and the metal-poor Galactic GC M13 (Simoda & Kimura 1968). The comparison LFs were scaled so that they had the same number of stars with  $21.4 \leq V \leq 25.5$  as the observed M31 halo LF did. In all four cases K-S tests returned less than a 17% confidence that the G302 field LF is drawn from one of the comparison single-metallicity populations. Fig. 8 show the LF for the G312 field and the same comparison LFs. K-S tests returned less than a 17% confidence that the G312 LF is drawn from

the same population as any of the comparison LFs.

It would be of interest to determine what fraction of the M31 halo stars belong to the metal-rich ( $[m/H] \sim -0.6$ ) population and what fraction belong to the metal-poor population that gives rise to the RR Lyrae stars. In order to estimate this ratio we modeled the observed LF of the M31 halo using a composite LF built from a metal-poor LF and a metal-rich LF. To model the metal-poor population we took the LF of the Galactic GC M13 (= NGC 6205), a typical metal-poor GC with  $[Fe/H] = -1.65$  (Zinn & West 1984). For the metal-rich population we used the observed LF of the M31 GC G1 from Rich et al. (1996). G1’s CMD suggests that cluster has a metallicity of  $[Fe/H] \simeq -0.6$  (Rich et al. 1996), significantly greater than the spectroscopic metallicity (Huchra et al. 1991) of  $[Fe/H] = -1.09$ . To determine the ratio of metal-poor to metal-rich stars we assumed that all the observed M31 halo stars with  $V < 22$  belonged to the metal-poor population. An examination of the CMDs (Figs. 4 and 5) shows no evidence for a significant number of RGB stars with metallicities less than this. We normalized the M13 LF to this number then scaled the G1 LF so that the total number of metal-poor and metal-rich stars (M13 LF + G1 LF) equaled the observed number of M31 halo stars with magnitudes of  $21.5 \leq V \leq 25.5$ . Fig. 9 shows the observed differential LF for the G302 field and the differential composite LF. Fig. 10 shows the same thing for the G312 field LF.

The observed number of stars drops relative to the composite LF when  $V \gtrsim 25.5$  suggesting that incompleteness is becoming significant at these magnitudes. K–S tests indicate that the composite LFs are the same as the observed LFs at the 99.97% confidence level for  $V \leq 25$  suggesting that the ratio of metal-rich to metal-poor populations is, broadly speaking, in agreement with the actual distribution in each field. The LFs were not compared at  $V > 25$  since there is the possibility that a second parameter affecting the morphology of the HB. In the G302 field the ratio of the metal-rich LF to the metal-poor LF is 3.58 : 1 while in the G312 field this ratio is 0.95 : 1. While it is tempting to conclude that that the G312 field contains a significantly different mix of stellar populations than the G302 field does it must be remembered that the metal-poor LF in our composite LF was scaled based on the (small) number of stars with  $21.5 \leq V \leq 22.5$ . Of the  $\sim 10$  stars observed in this magnitude range in the G302 field  $\sim 2$  will be foreground stars (Ratnatunga & Bahcall 1985) and some will be AGB stars. These effects, and Poisson uncertainties, will introduce uncertainties of  $\sim 50\%$  into the derived metallicity ratios.

The large uncertainties in our composite LFs make us hesitant to make any definite statements as to whether or not the stellar populations in our two fields are the same. The composite LFs in the two fields are the same at only the 9.8% confidence level, however the RGB and HB morphologies and metallicity distributions all suggest that the G302 field and G312 field contain the same stellar populations. We do not, therefore, believe that our analysis conclusively demonstrates that the G302 field contains a different mix of stellar populations than the G312 field does but we stress that this is not a strong conclusion and that further work will be needed in many different halo fields to determine what, if any, variation between position and population exists in the halo of M31. We do, however, believe that this analysis demonstrates that a non-negligible

fraction ( $\sim 25\%$  to  $50\%$ ) of the halo of M31 *in our fields of study* is made up of metal-poor stars that may give rise to the observed RR Lyrae variables.

## 5. Conclusions

We used *HST* WFPC2 *V*- and *I*-band photometry to show that the stellar halo of M31 has a mean metallicity of  $[m/H] \simeq -0.6$  with a spread of  $-2 \lesssim [m/H] \lesssim -0.2$ , comparable to the metallicity determinations made using ground-based observations. This result is primarily based on a comparison of the morphology of the RGB to fiducial sequences of Galactic GCs and theoretical RGB isochrones. The HB consists primarily of red clump stars, similar to what is seen in 47 Tuc, and a small number of blue stars. A metallicity of  $[m/H] \simeq -0.6$ , the observed metallicity spread in the RGB, and the observed distribution of stellar luminosities on the HB is consistent with the Chaboyer et al. (1996) relationships between the metallicity and absolute magnitudes of RR Lyrae variables. The horizontal branch morphology ratio is  $(N_B - N_R)/(N_B + N_R) \simeq -0.9$ , suggesting that there is a metal-poor population present that could give rise to the RR Lyrae variables seen by Pritchett & van den Bergh (1987). The derived helium abundance is  $Y \simeq 0.20$  to  $0.27$ , similar to that in Galactic GCs.

Combining LFs from metal-rich and metal-poor populations and comparing the resulting composite LF to the observed LF for the M31 halo suggests that metal-rich ( $[m/H] \simeq -0.6$ ) stars make up between half and three-quarters of the M31 halo in each of our fields while the remaining stars belong to a metal-poor population with  $[m/H] \sim -1.5$  to  $-2.0$ . The metallicity distributions of HB and RGB stars are both consistent with such a mix of metal-rich and metal-poor stars. The HB, however, is redder than would be expected given this mix of metallicities. This may be due to blue HB stars being too faint to appear in our data or it may indicate that a second parameter is affecting the HB morphology in the halo of M31.

We find no conclusive evidence for a difference in stellar population between the G302 field and the G312 field. LFs suggest that the G312 ( $R_{M31} = 50'$ ) field may contain a higher fraction of metal-poor stars than the G302 ( $R_{M31} = 32'$ ) field but the metallicity distribution of RGB stars indicates that there is no significant difference in the ratio of metal-rich to metal-poor stars in the two fields. Deep photometry will be needed in a large number of fields in the M31 halo to determine how (or if) metallicity varies with position in the halo of M31.

This research is based on observations made with the NASA/ESA *Hubble Space Telescope* obtained at the Space Telescope Science Institute. STScI is operated by the Association of Universities for Research in Astronomy Inc. under NASA contract NAS 5-26555. Support for this research was provided by operating grants to GGF and HBR from the Natural Science and Engineering Research Council of Canada. SH would like to thank Peter Stetson for kindly making a copy of the ALLFRAME software available. We would also like to thank the referee, René Racine,

for making several useful suggestions.

## REFERENCES

- Ashman, K. M., & Bird, C. M. 1993, *AJ*, 106, 2281
- Bahcall, J. N., & Soneira, R. M. 1984, *ApJS*, 55, 67
- Bergbusch, P. A., & Vandenberg, D. A. 1992, *ApJS*, 81, 163
- Bertelli, G., Bressan, A., Chiosi, C., Fagotto, F., & Nasi, E. 1994, *A&AS*, 106, 275
- Bessell, M. S., & Brett, J. M. 1988, *PASP*, 100, 1134
- Bohlin, R. C., Deutsch, E. W., McQuade, K. A., Hill, J. K., Landsman, W. B., O’Connell, R. W., Roberts, M. S., Smith, A. M., Stecher, T. P. 1993, *ApJ*, 417, 127
- Brewer, J. P., Richer, H. B., Crabtree, D. R. 1995, *AJ*, 109, 2480
- Burstein, D., & Heiles, C. 1982, *AJ*, 87, 1165
- Burstein, D., Faber, S. M., Gaskell, C. M., & Krumm, N. 1984, *ApJ*, 287, 586
- Buzzoni, A., Fusi Pecci, F., Buonanno, R., & Corsi, C. E. 1983, *A&A*, 128, 94
- Carney, B. W., Storm, J., & Jones, R. V. 1992, *ApJ*, 386, 663
- Chaboyer, B., Demarque, P., & Sarajedini, A. 1996, *ApJ*, 459, 558
- Christian, C. A., & Heasley, J. N. 1991, *AJ*, 101, 848
- Couture, J., Racine, R., Harris, W. E., & Holland, S. 1995, *AJ*, 109, 2050
- Crotts, A. P. S. 1986, *AJ*, 92, 292
- Da Costa, G. S., & Armandroff, T. E. 1990, *AJ*, 100, 162
- Davidge, T. J. 1993, *ApJ*, 409, 190
- de Vaucouleurs, G. 1958, *ApJ*, 128, 465
- Durrell, P. R., Harris, W. E., & Pritchett, C. J. 1994, *AJ*, 108, 2114
- Faber, S. 1995, in *Stellar Populations*, eds. L. G. Gilmore, & P. van der Kruit, (Dordrecht, Kluwer), IAU Symp. 169, (in press)
- Freedman, W. L., & Madore, B. F. 1990, *ApJ*, 365, 186
- Frogel, J. A., Persson, S. E., & Cohen, J. G. 1980, *ApJ*, 240, 785
- Grillmair, C. J., Freeman, K. C., Irwin, M., & Quinn, P. J. 1995, *AJ*, 109, 2553
- Hesser, J. E., Harris, W. E., Vandenberg, D.A., Allwright, J. W. B., Shott, P., & Stetson, P. B. 1987, *PASP*, 99, 739
- Hodder, P. J. C. 1995, PhD. Thesis, UBC
- Hodge, P. 1992, *The Andromeda Galaxy*, (Dordrecht, Kluwer)

- Holland, S. 1997, PhD. Thesis, in preparation
- Holland, S., Fahlman, G. G., & Richer, H. B. 1996, in preparation
- Holtzman, J. A., et al. 1995a, PASP, 107, 156
- Holtzman, J. A., Burrows, C. J., Casertano, S., Hester, J. J., Trauger, J. T., Waterson, A. M., & Worthey, G. S. 1995b, PASP, 107, 1065
- Huchra, J. P., Brodie, J. P., & Kent, S. M. 1991, ApJ, 370, 495
- Ibata, R. A., Cilmore, G. G., & Irwin, M. J. 1994, Nature, 370, 194
- King, I. R. 1966, AJ, 71, 64
- Lee, S.-W. 1977, A&AS, 27, 381
- Lee, Y.-K., Demarque, P., & Zinn, R. 1994, ApJ, 423, 248
- Lin, D. H., & Richer, H. B. 1992, ApJ, 388, L57
- Michie, R. W. 1963, MNRAS, 125, 127
- Moffat, A. F. J. 1969, A&A, 3, 455
- Mould, J., & Kristian, J. 1986, ApJ, 305, 591
- Peacock, J. A. 1983, MNRAS, 202, 615
- Pritchett, C. J. & van den Bergh, S. 1987, ApJ, 316, 517
- Pritchett, C. J., & van den Bergh, S. 1988, ApJ, 331, 135
- Pritchett, C. J. & van den Bergh, S. 1994, AJ, 107, 1730
- Ratnatunga, K. U., & Bahcall, J. N. 1985, ApJS, 59, 63
- Rich, R. M., & Mighell, K. J. 1995, ApJ, 439, 145
- Rich, R. M., Mighell, K. J., Freedman, W. L., & Neill, J. D. 1996, AJ 111, 768
- Richer, H. B., Harris, W. E., Fahlman, G. G., Bell, R. A., Bond, H. E., Hesser, J. E., Holland, S., Pryor, C., Stetson, P. B., Vandenberg, D. A., & van den Bergh, S. 1996, ApJ, 463, 602
- Sarajedini, A., & Layden, A. C. 1995, AJ, 109, 1086
- Simoda, M. & Kimura, H. 1968, ApJ, 151, 133
- Smail, I., Hogg, D. W., Yan, L., & Cohen, J. G. 1995, ApJ, 449, L105
- Stetson, P. B. 1987, PASP, 99, 191
- Stetson, P. B. 1994, PASP, 106, 250
- Stetson, P. B. 1996, private communication
- Tripicco, M. J. 1989, AJ, 97, 735
- van den Bergh, S. 1991, PASP, 103, 1053
- van den Bergh, S. 1993, ApJ, 411, 178



Zinn, R. & West, M. 1984, ApJS, 55, 45

Table 1. Log of the Observations.

Field	Date (1995)	Filter	Exposure (s)
G302	Nov. 5	F555W	$8 \times 500$
			$2 \times 160$
		F814W	$7 \times 500$
			$1 \times 400$
			$1 \times 160$
G312	Oct. 31	F555W	$8 \times 500$
			$2 \times 160$
		F814W	$7 \times 500$
			$1 \times 400$
			$1 \times 160$

Table 2. Aperture Corrections.

Field	CCD	Filter	$\langle \text{ap} - \text{PSF} \rangle$	Slope	N
G302	WF2	F555W	$+0.0184 \pm 0.0216$	1.065	25
		F814W	$+0.0374 \pm 0.0099$	1.017	80
	WF4	F555W	$+0.0333 \pm 0.0119$	1.011	90
		F814W	$+0.0297 \pm 0.0053$	1.005	252
G312	WF2	F555W	$-0.0344 \pm 0.0144$	1.008	186
		F814W	$+0.0405 \pm 0.0087$	1.034	119
	WF4	F555W	$+0.0513 \pm 0.0165$	1.001	85
		F814W	$+0.0333 \pm 0.0102$	1.027	89

Table 3. Photometric Uncertainties.

$V$	G302F $\sigma_V$	G312F $\sigma_V$	$I$	G302F $\sigma_I$	G312F $\sigma_I$
20.25	0.035	0.033	20.25	0.033	0.028
20.75	0.033	0.038	20.75	0.028	0.029
21.25	...	0.031	21.25	0.030	0.028
21.75	0.050	0.035	21.75	0.031	0.031
22.25	0.043	0.038	22.25	0.034	0.034
22.75	0.039	0.042	22.75	0.041	0.040
23.25	0.045	0.045	23.25	0.049	0.048
23.75	0.053	0.053	23.75	0.061	0.060
24.25	0.062	0.061	24.25	0.075	0.073
24.75	0.076	0.076	24.75	0.100	0.100
25.25	0.091	0.090	25.25	0.142	0.144
25.75	0.121	0.122	25.75	0.208	0.205
26.25	0.165	0.166	26.25	0.299	0.304
26.75	0.235	0.241	26.75	0.463	0.459
27.25	0.344	0.346	27.25	0.752	0.677
27.75	0.547	0.492	27.75	...	...

Table 4. The  $V$ - and  $I$ -band apparent LFs.

$V$	$\phi_V$ G302F	$\phi_V$ G312F	$I$	$\phi_I$ G302F	$\phi_I$ G312F
20.00	0	0	20.00	2	0
20.20	2	0	20.20	4	2
20.40	1	1	20.40	8	4
20.60	1	0	20.60	17	9
20.80	0	0	20.80	35	5
21.00	1	1	21.00	42	9
21.20	0	0	21.20	53	12
21.40	0	1	21.40	49	9
21.60	2	1	21.60	46	9
21.80	4	3	21.80	49	11
22.00	9	3	22.00	71	25
22.20	8	6	22.20	69	18
22.40	20	5	22.40	113	28
22.60	29	10	22.60	89	28
22.80	45	8	22.80	121	30
23.00	65	10	23.00	154	42
23.20	78	20	23.20	194	52
23.40	106	36	23.40	174	45
23.60	123	25	23.60	225	44
23.80	180	46	23.80	304	68
24.00	168	52	24.00	555	138
24.20	222	52	24.20	1204	275
24.40	217	52	24.40	987	237
24.60	263	58	24.60	586	145
24.80	478	115	24.80	418	106
25.00	953	259	25.00	388	110
25.20	1260	275	25.20	357	115
25.40	674	144	25.40	346	110
25.60	476	122	25.60	319	96
25.80	436	125	25.80	290	102
26.00	419	126	26.00	254	90
26.20	398	129	26.20	185	78
26.40	355	98	26.40	81	43
26.60	300	101	26.60	43	23
26.80	257	86	26.80	13	5

Table 4—Continued

$V$	$\phi_V$		$I$	$\phi_I$	
	G302F	G312F		G302F	G312F
27.00	150	77	27.00	5	4
27.20	97	40	27.20	0	1
27.40	40	31	27.40	1	0
27.60	14	11	27.60	0	0
27.80	6	2	27.80	0	0
28.00	1	1	28.00	0	0

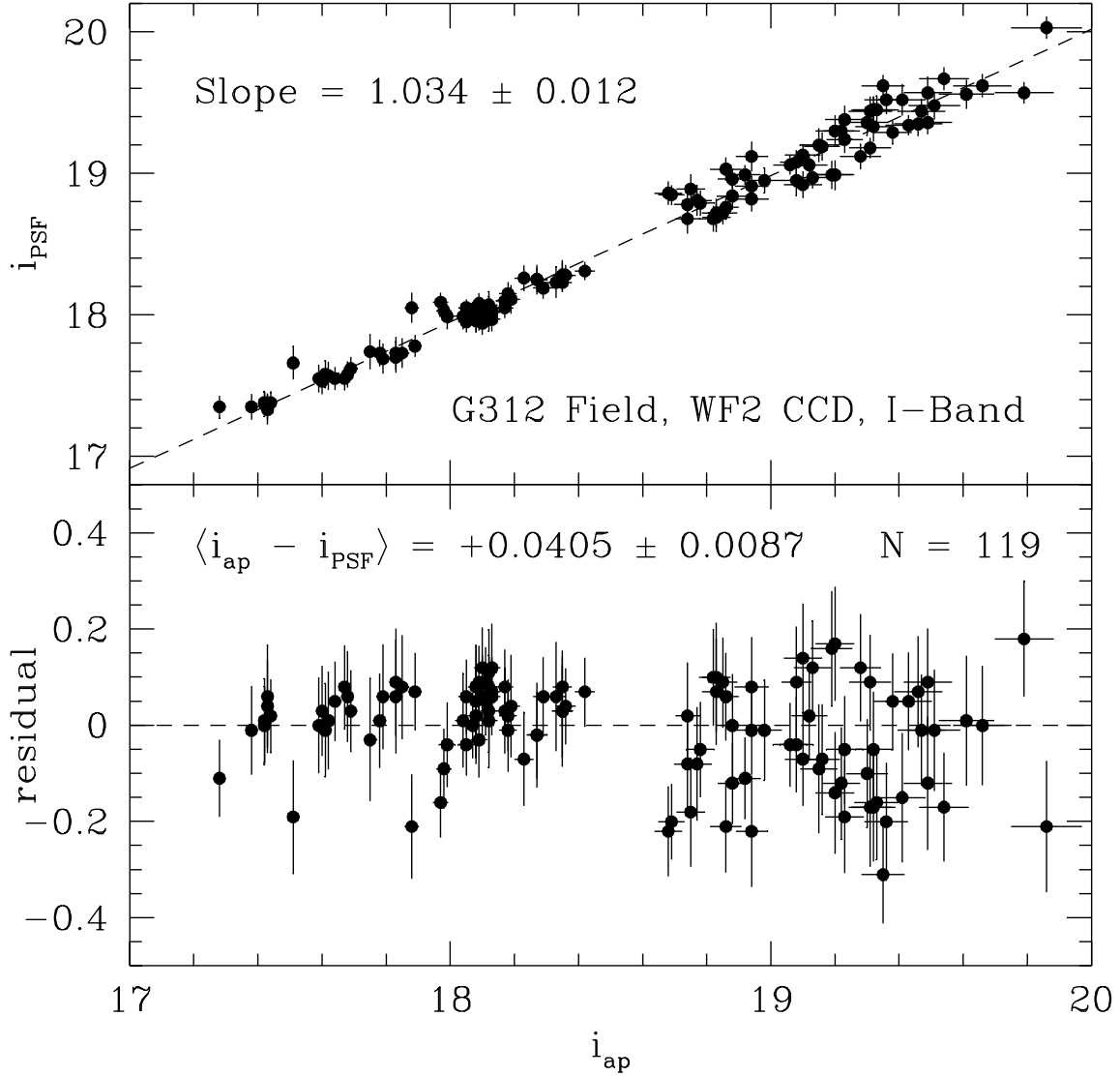


Fig. 1.— The upper panel shows the aperture-magnitude vs PSF-magnitude relation for the *I*-band photometry from the WF2 CCD in the G302 field. Stars were discarded until the slope of this relation approached unity. The lower panel show the residuals ( $= (v_{\text{ap}} - v_{\text{PSF}}) - \Delta v$ , where  $\Delta v = \langle v_{\text{ap}} - v_{\text{PSF}} \rangle$ ). Stars that failed the culling process described in Sec. 2.2 have not been plotted.

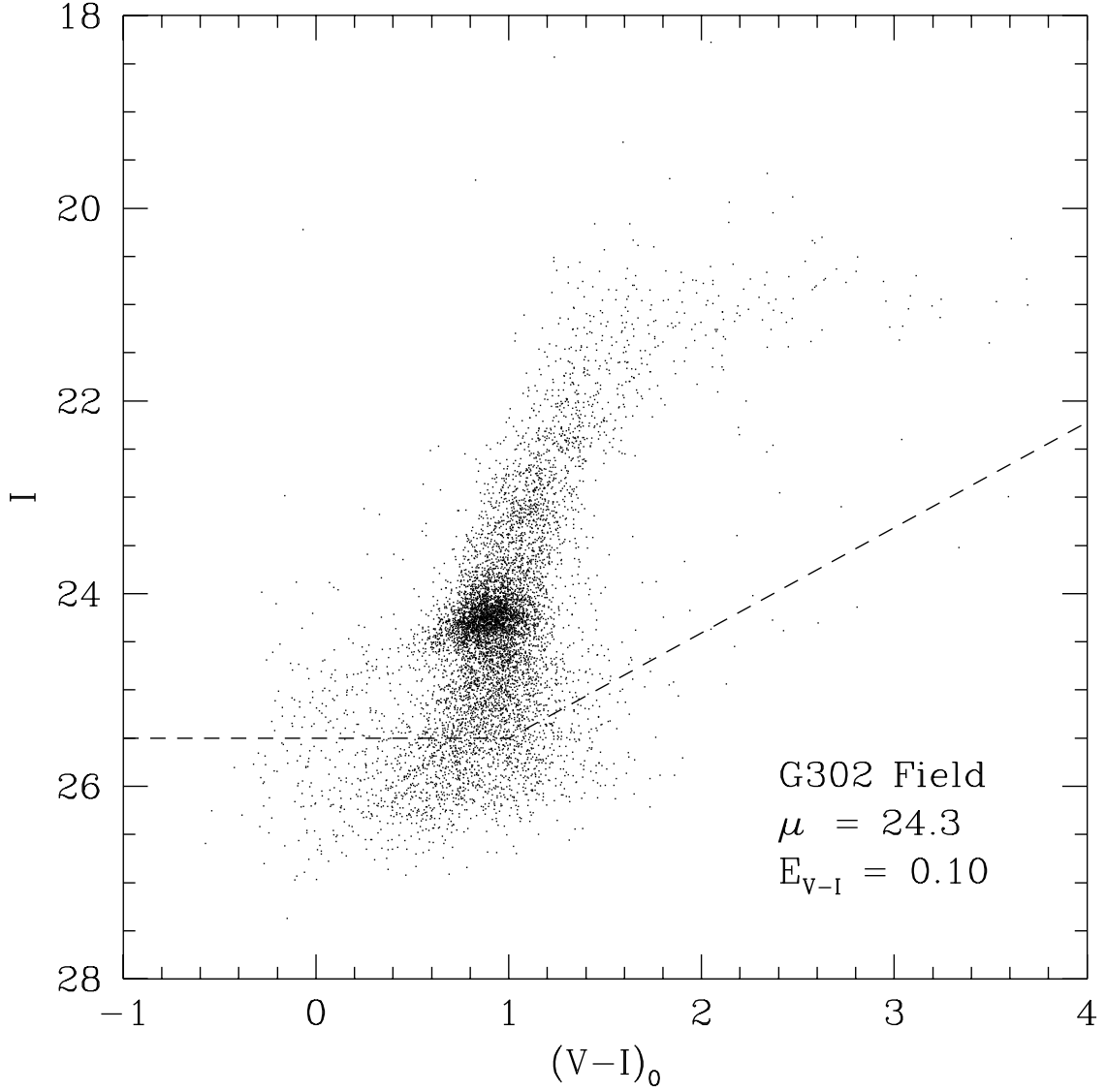


Fig. 2.— This Fig. shows the CMD for the M31 halo field around the GC G302. This diagram shows all star-like sources in our images. No attempt has been made to remove foreground or background contamination. The dashed line shows the location where the photometric uncertainties are  $\sigma_{(V-I)} \simeq 0.2$ . We believe that this also corresponds to the approximate location where our data becomes incomplete. The distance modulus and extinction quoted are the values that were used to calibrate our photometry (see Holtzman et al. 1995b).

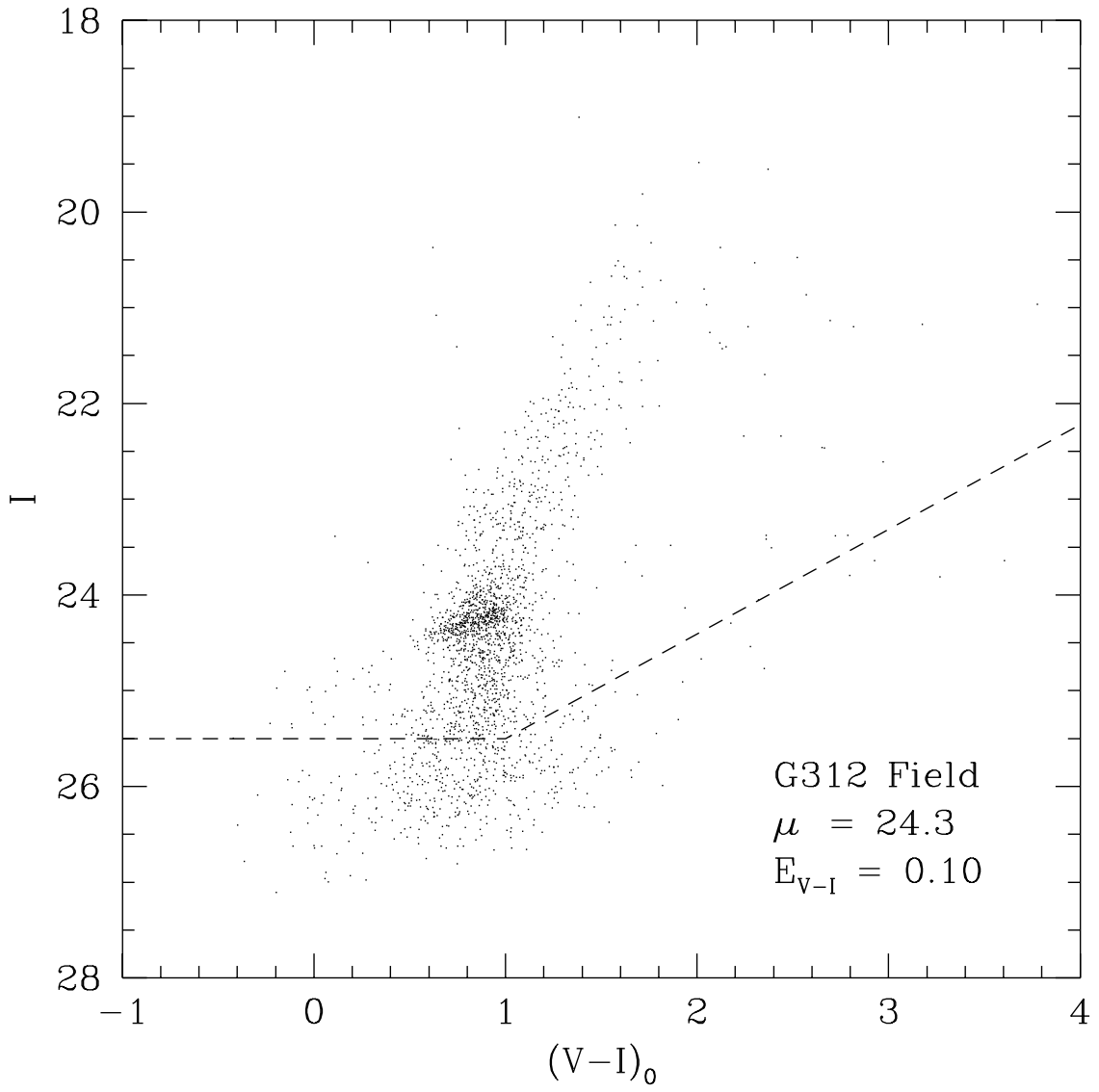


Fig. 3.— This Fig. is the same as Fig. 2 but shows the CMD for the M31 halo field around the GC G312.



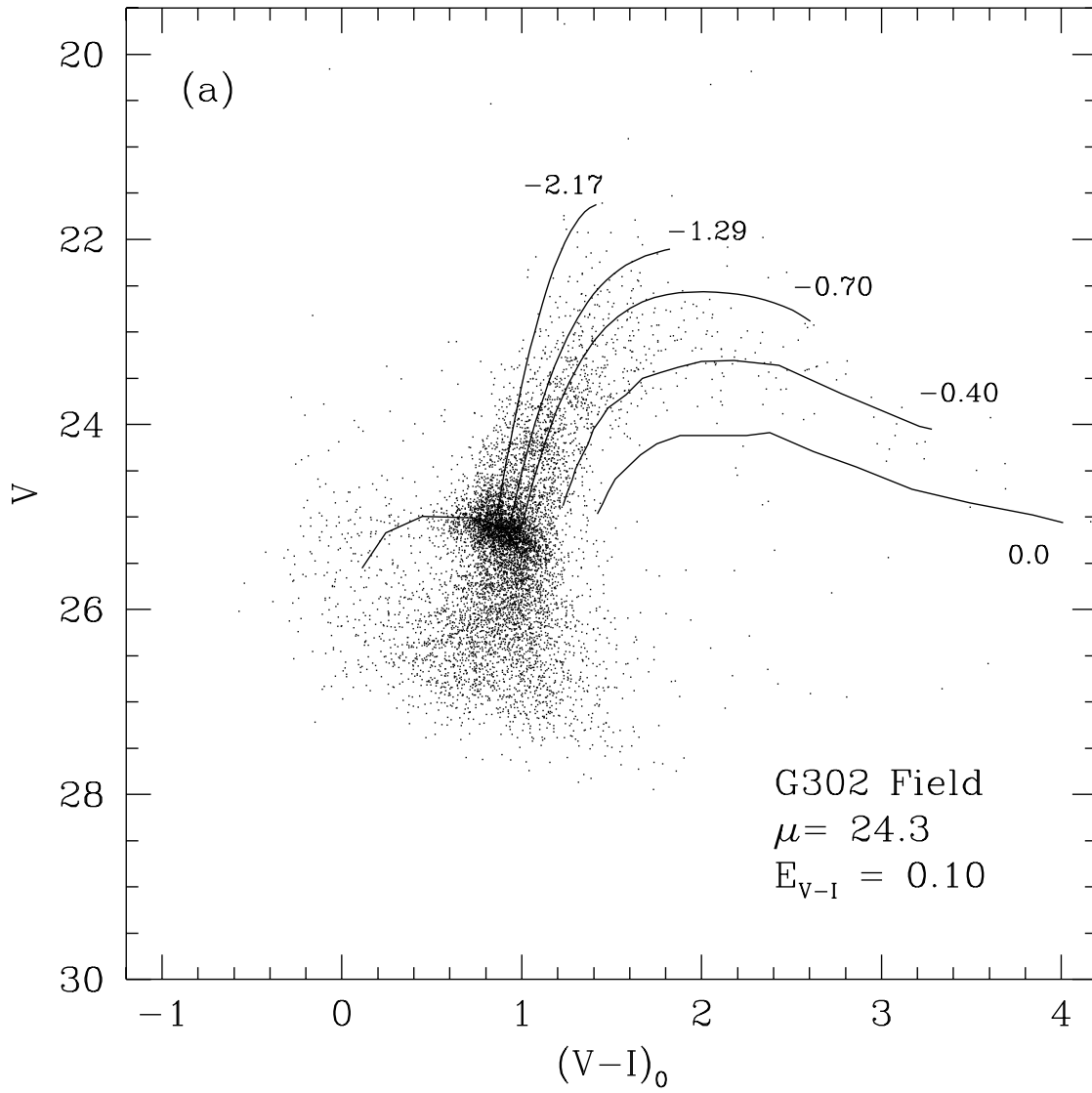


Fig. 4.— This Fig. shows the CMD for stars in the WF2 and the WF4 CCDs in the G302 field. The fiducial sequences are described in Sec. 3.2.

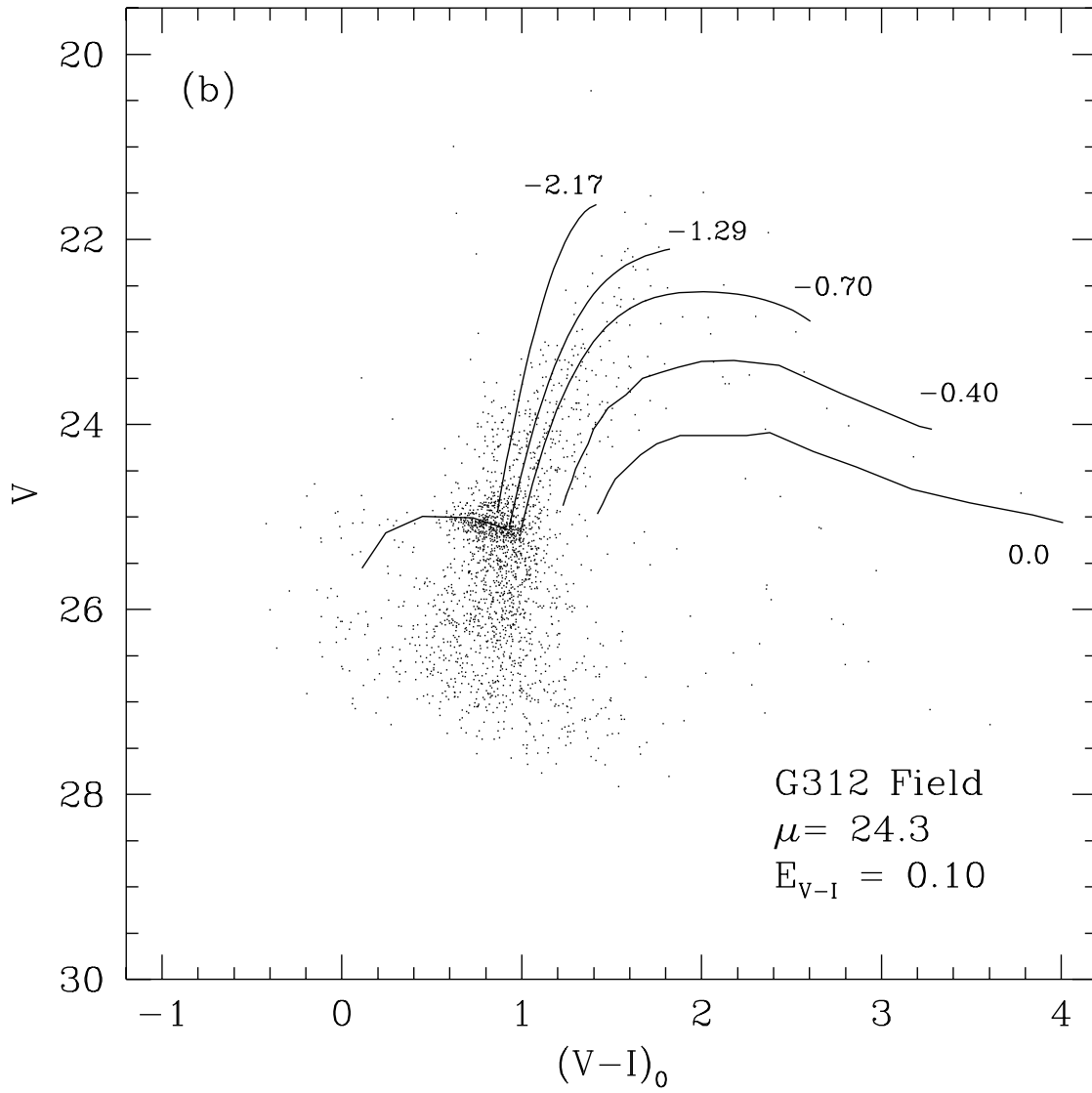


Fig. 5.— This Fig. shows the CMD for stars in the WF2 and the WF4 CCDs in the G312 field. The fiducial sequences are described in Sec. 3.2.

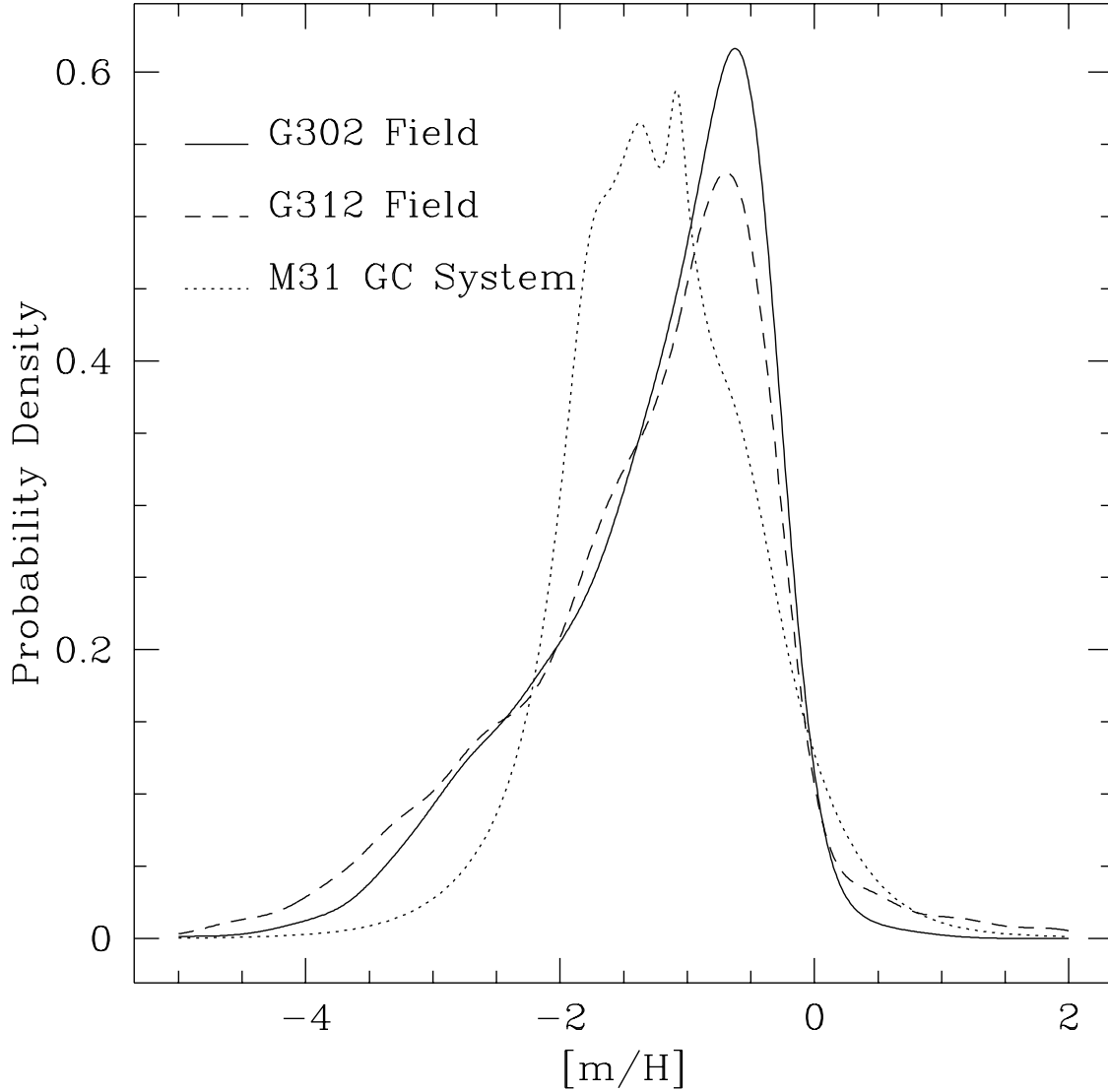


Fig. 6.— The probability density distribution for the metallicity of RGB stars in the G302 field (solid line), the G312 field (dashed line), and for the M31 GC system (dotted line). For each star we generated a unit Gaussian with a standard deviation of  $\sigma = 0.25$  dex, the estimated uncertainty in the metallicity determination for an individual star. For the GC distribution the individual  $\sigma_{[\text{Fe}/\text{H}]}$  values from Huchra et al. (1991) were used. The normalized sum of these Gaussians is a non-parametric histogram of the probability density,  $P([\text{m}/\text{H}])$ , distribution. The sharp red edge in the distribution suggests that there is a well-defined upper limit to the metallicity of stars in the G302 and G312 fields while the slow decline on the blue edge suggests that the metal-poor stars cover a range of metallicities. A portion of the metal-poor tail arises from the confusion of AGB stars with metal-poor RGB stars.

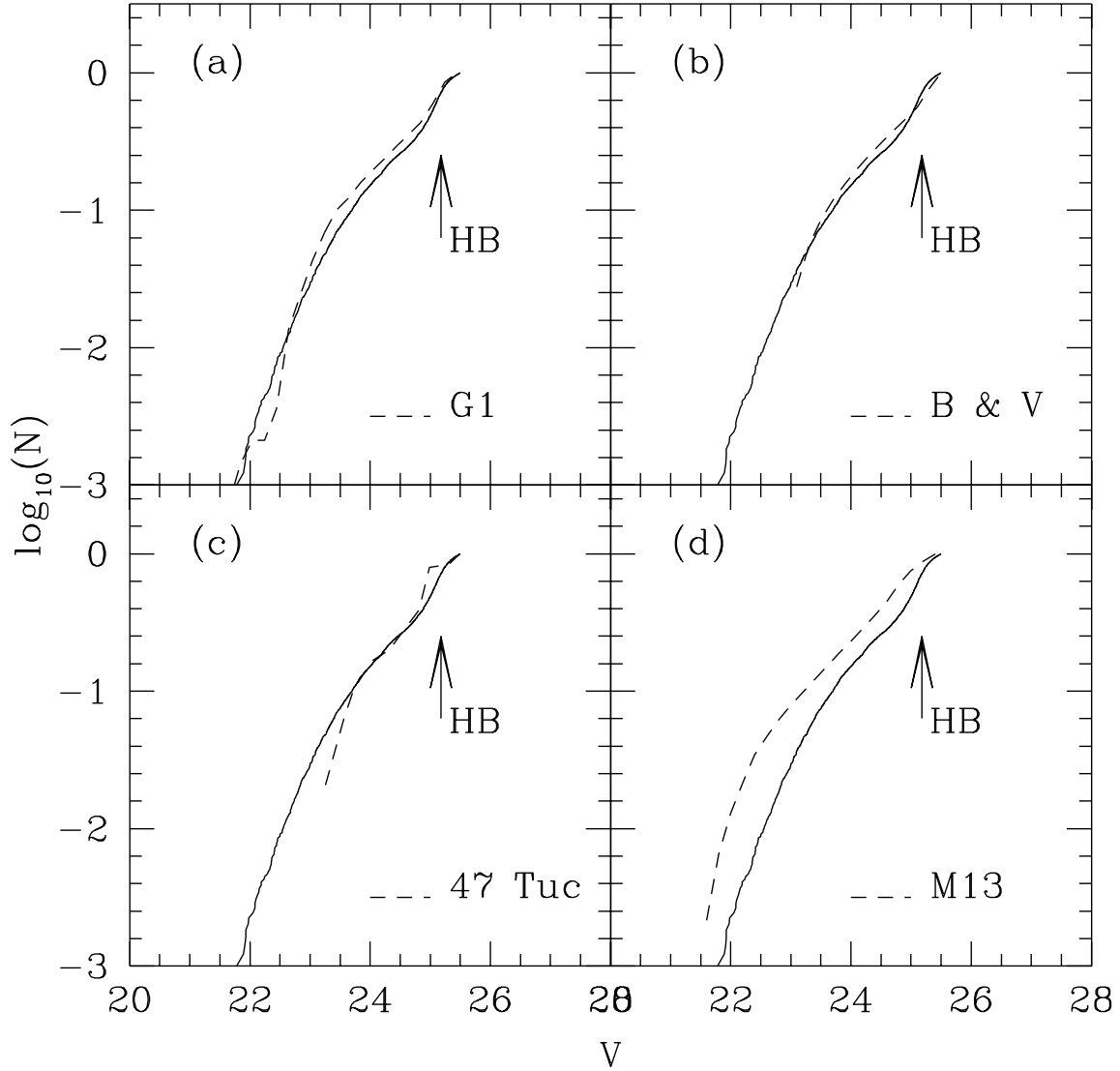


Fig. 7.— Here we compare the cumulative LF for the M31 halo field near G302 (solid lines) with four comparison LFs (dashed lines: (a) the G1 LF, (b) a theoretical LF (B & V) with  $[\text{Fe}/\text{H}] = -0.47$ ,  $[\text{O}/\text{Fe}] = +0.23$  and  $t_0 = 14$  Gyr, (c) the 47 Tuc LF, and (d) the M13 LF. The comparison LFs were scaled so that the total number of stars with  $21 \leq V \leq 25.5$  was the same as the number of stars in the G302 field in the same range of magnitudes.  $V = 25.5$  was selected as the faint cut-off because we believe our photometry is reasonably complete down to approximately this point (see Sec. 4).

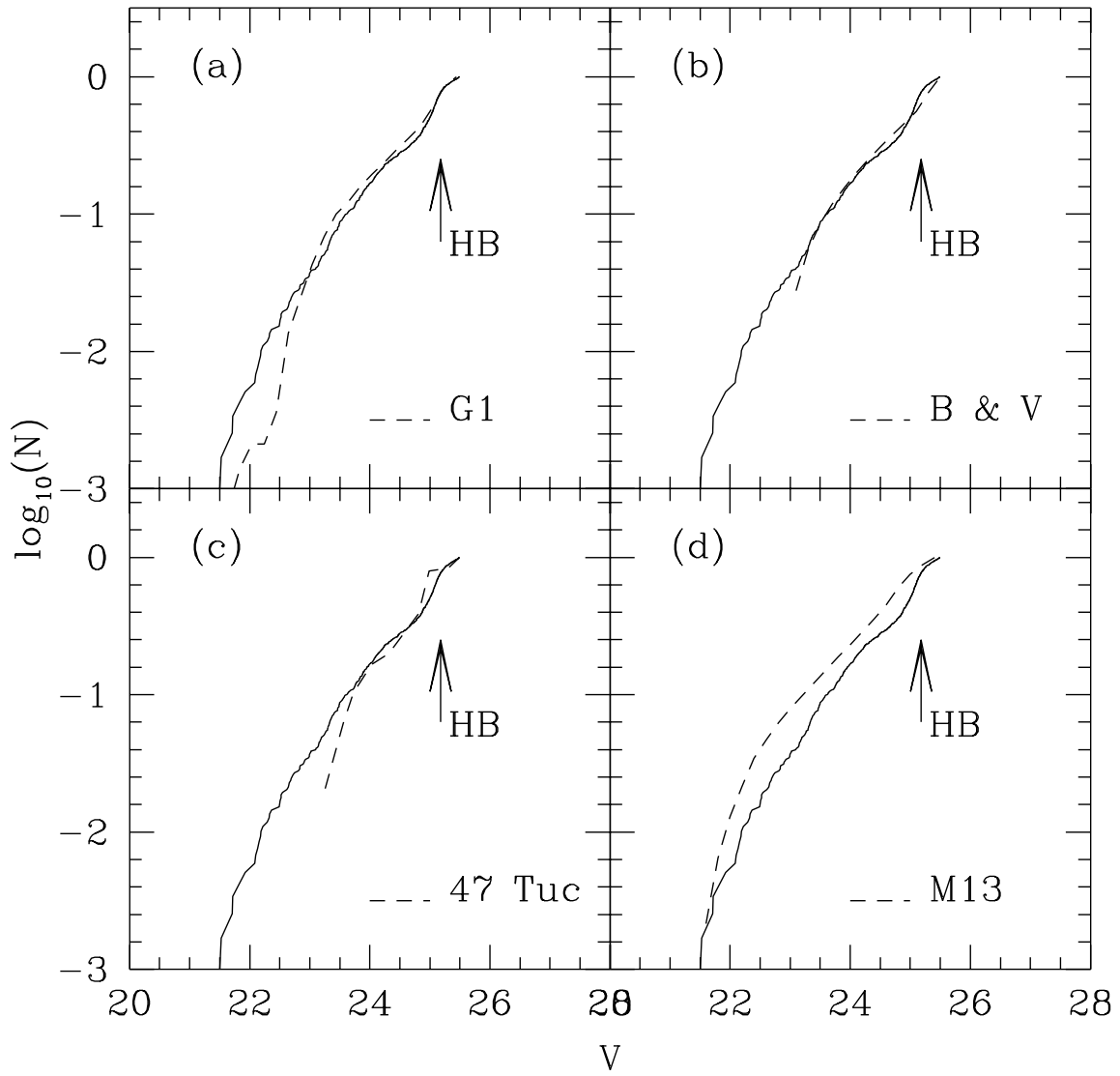


Fig. 8.— Here we compare the cumulative LF for the M31 halo field near G312 with the four comparison LFs used in Fig. 7.

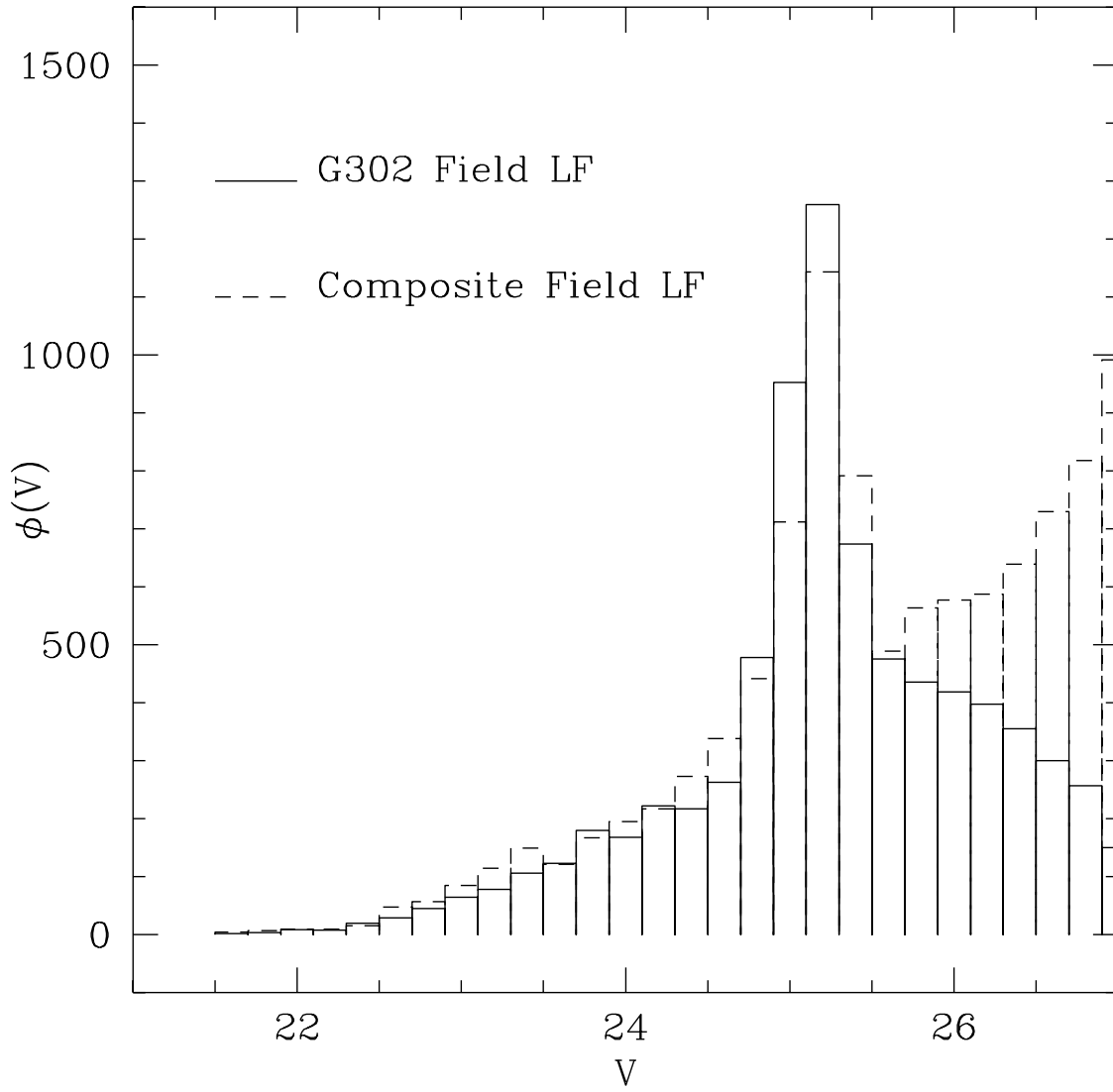


Fig. 9.— The observed LF in the G302 field and the composite LF built from scaling the G1 and M13 LFs as described in Sec. 4. The poor agreement at  $V \gtrsim 25.5$  may be due to incompleteness in the observed LF.

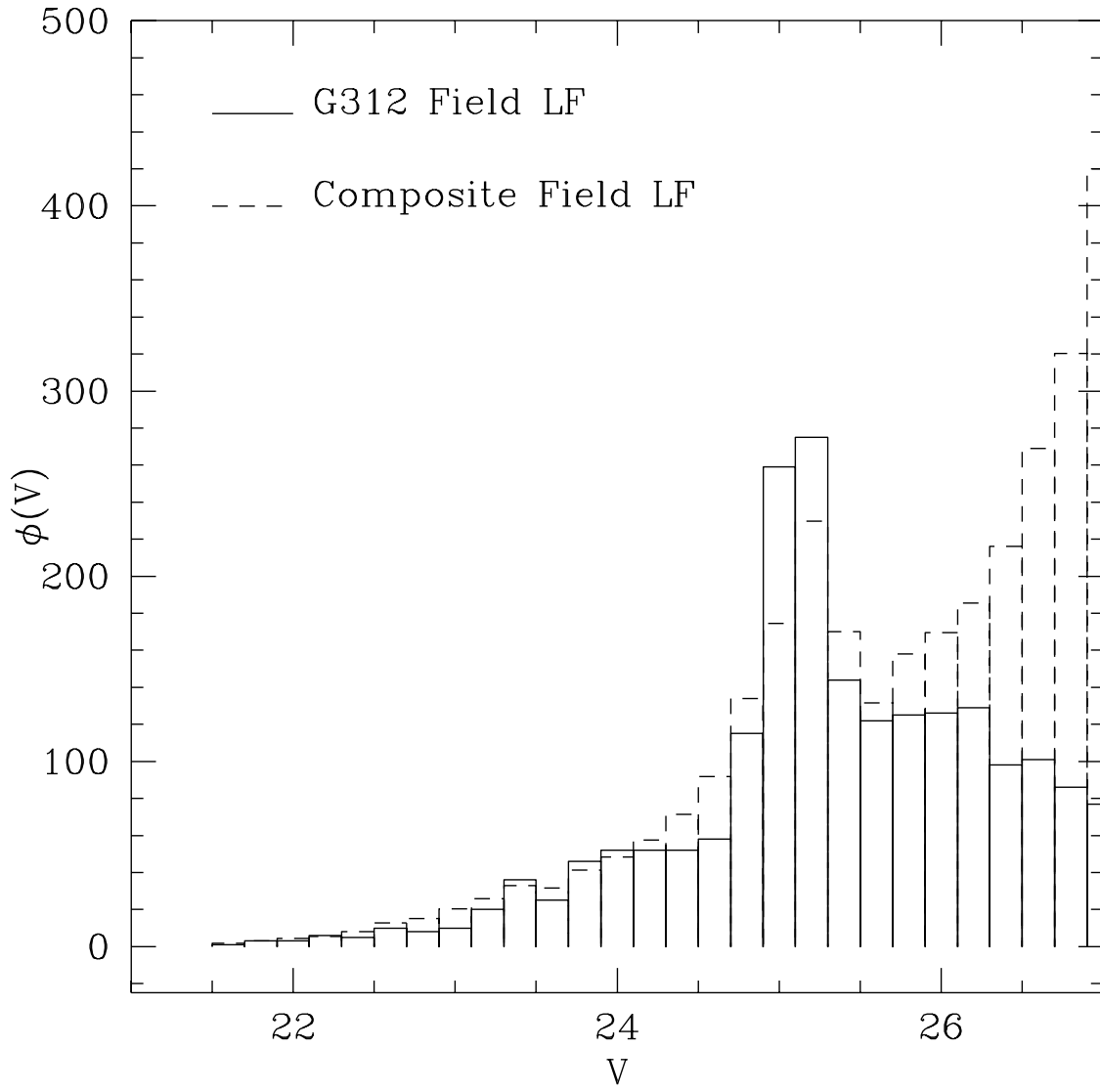


Fig. 10.— The same as Fig. 9 but for the G312 field LF.